PROCEEDINGS, 48th Workshop on Geothermal Reservoir Engineering
Stanford University, Stanford, California, February 6-8, 2023
SGP-TR-224

Stochastic Inversion of Gravity and Magnetic Data to Build Subsurface Geological Fault Models Using Evolution and Swarm Intelligence-Inspired Optimization Algorithms

Divakar Vashisth[1], Ahinoam Pollack[1], Tapan Mukerji[1] and Drew Siler[2,3]

[1]Department of Energy Science and Engineering, Stanford University, CA, USA

[2]Geology, Minerals, Energy, and Geophysics Science Center, U.S. Geological Survey, Moffett Field, CA, USA

[3]Current Affiliation: Geologica Geothermal Group, Reno, NV, USA

divakar.vashisth98@gmail.com

Keywords: stochastic inversion, uncertainty analysis, geological fault models, sensitivity analysis, differential evolution, genetic algorithm, particle swarm optimization, grey wolf optimization

ABSTRACT

Geothermal energy will play an important role in supplying heat and electricity to meet the demands of a low-carbon future. The exploration stage of a geothermal system involves acquiring geological, geophysical, and wellbore or flow-related data. These data are subject to a variety of modeling and inversion techniques that help constrain geologic structure and hydrothermal processes. The non-uniqueness of such inversion adds uncertainty to subsurface interpretations, because multiple models can give a good match with the observed data. Since permeable faults carrying hydrothermal fluids are relatively rare in the subsurface, this uncertainty can increase the financial risk of well drilling and geothermal development. We aim to study this subsurface uncertainty by inverting gravity and magnetic data using stochastic global optimization techniques.

In this paper, we implemented a synthetic study to get a better understanding of the inversion algorithms, data sensitivity to model parameters, and the impact of acquiring dense versus sparse data. We generated a three-dimensional four-layered earth model (inspired by the Bradys geothermal field) with five faults and simulated synthetic gravity and magnetic data. The earth model was defined by a set of model parameters that include density, magnetic susceptibility, and thickness of each layer, and a number of fault parameters like fault location, deformation ellipse properties, dip, dip direction, and slip on each fault. The objective was to invert both the data types individually and get a suite of models that when forward modeled fit well with the observed ("true") data. The inversion was carried out using two evolution-inspired (genetic algorithm and differential evolution) and two swarm intelligence-inspired (grey wolf optimizer and particle swarm optimizer) global optimization techniques followed by a comparison between the results of these algorithms and the true model. Distance-based global sensitivity analysis of gravity and magnetic data to the model parameters was also performed to validate the results of inversion, as the model parameter to which a data type is highly sensitive is likely to have reduced uncertainty after inversion. We demonstrated that gravity and magnetic inversion reduced uncertainty on both lithological and structural subsurface parameters. In addition, dense and sparse acquisition grids were compared for uncertainty reduction of model parameters following inversion.

1. INTRODUCTION

Potential field surveys such as gravity and magnetics are widely used in groundwater, thermal water, mineral, hydrocarbon, and geothermal exploration (Grant and West, 1965; Telford et al., 1976; Serpa and Cook, 1984; Baillieux et al., 2013; Martinez and Li, 2015; Tontini et al., 2016). The economical aspects of the data acquisition and the density and magnetic susceptibility contrasts due to the subsurface displacements along the faults make these potential field methods viable for geothermal exploration. Serpa and Cook (1984) performed inversion of gravity and aeromagnetic data to study a geothermal field in Utah. Witter et al. (2016a) inverted gravity data to test a 3D geological model of the Bradys geothermal field. Witter et al. (2016b) used gravity data to aid geothermal exploration in Hot Springs Bay Valley Area in Alaska, and Witter et al. (2017) made use of ground magnetic data for geothermal subsurface modeling at Baker Hot Springs. Lewerissa et al. (2020) carried out inversion of gravity and magnetic data to evaluate geothermal system in Suli and Tulehu, while Ardestani et al. (2021) investigated (processed and inverted) gravity and magnetic data over the Mahallat Geothermal System to explore the geological features and geothermal system manifestations. Pollack et. al. (2021) performed stochastic inversion of gravity, magnetic and other data types to create geologically realistic structural models for the Patua Geothermal Field. Calderon and Gallardo (2022) inverted gravity and magnetic data from Acoculco geothermal zone in Mexico to identify potential low-permeability geothermal reservoirs, and Carrillo et al. (2022) performed joint inversion of gravity and magnetic data from the Los Humeros geothermal field in Mexico to generate 3-D subsurface models.

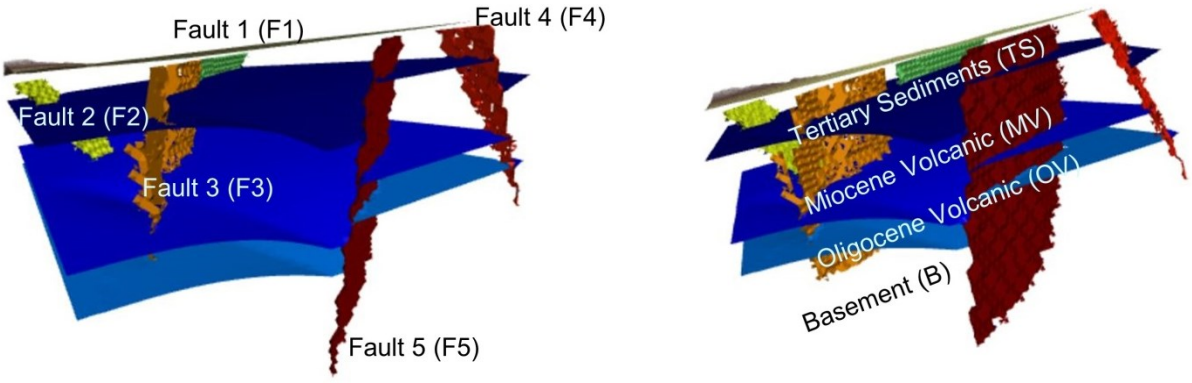

Figure 1: Synthetic four-layered, five-fault earth model used in this study depicted from different view angles.

One of the major barriers for geothermal development is financial risk due to geological uncertainty. Drilling wells is very costly, and a well will only produce if it intersects a permeable fault carrying hydrothermal fluids. Very similar gravity and magnetic data can be observed over different geological fault models. A single incorrect geological model obtained from deterministic inversion can lead to a well missing the fault, so an ensemble of earth models is required to compute the uncertainty in fault location and parameters. Uncertainty quantification can aid in evaluating the risk of drilling a "dry well" and communicating that risk with investors and insurance companies.

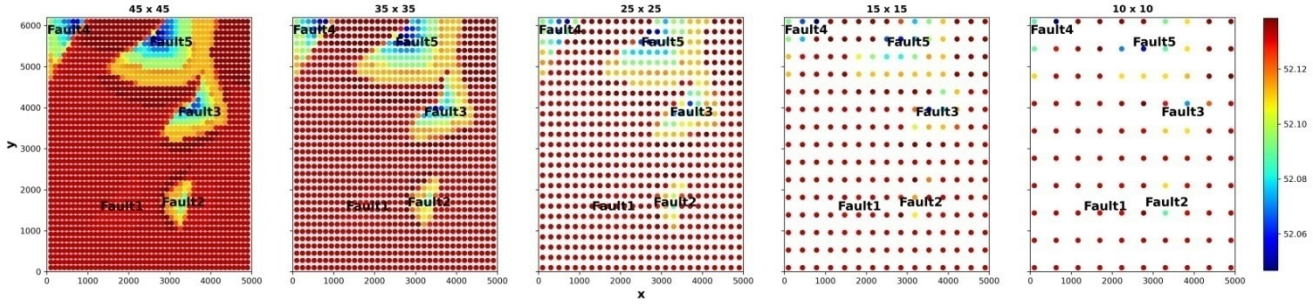

Figure 2: Simulated gravity data in plan view over the synthetic geological fault model (Figure 1) for different acquisition scenarios- (a) 45x45, (b) 35x35, (c) 25x25, (d) 15x15, and (e) 10x10 acquisition grids.

A number of stochastic global optimization algorithms like simulated annealing (Kirkpatrick et al. 1983; Sen and Stoffa, 1991; Ma, 2001; Beaty et al. 2002; Ryden and Park, 2006; Yin and Hodges, 2007), genetic algorithm (Holland, 1975; Sambridge, 1992; Sen et al., 1995; Ramillien, 2001; Tarantola, 2005; Xing and Mazzotti, 2019), differential evolution (Storn and Price, 1995; Storn and Price, 1997; Růžek and Kvasnička, 2001; Qing, 2009; Saraswat et al., 2010; Li and Yin, 2012; Balkaya, 2013; Pan et al., 2018; Roy et al., 2021), particle swarm optimization (Kennedy and Eberhart, 1995; Shaw and Srivastava, 2007; Martinez et al., 2010; Liu et al., 2018; Pace et al., 2021), grey wolf optimization (Mirjalili et al., 2014; Song et al., 2015; Chandra et al., 2017; Agarwal et al., 2018; Vashisth and Shekar, 2019; Sharma et al., 2021, Vashisth et al., 2022), whale optimization algorithm (Mirjalili and Lewis, 2016; Vashisth et al., 2018; Abdelazeem, 2019; Vashisth et al., 2019) and many more have been used to solve a variety of geophysical inverse problems. Easy implementation and flexible applicability without the need for derivatives make these algorithms popular in solving a wide range of problems. We make use of the stochastic nature of some of the above-mentioned derivative-free optimization algorithms to generate an ensemble of realistic geologic structural models from gravity and magnetic data inversion.

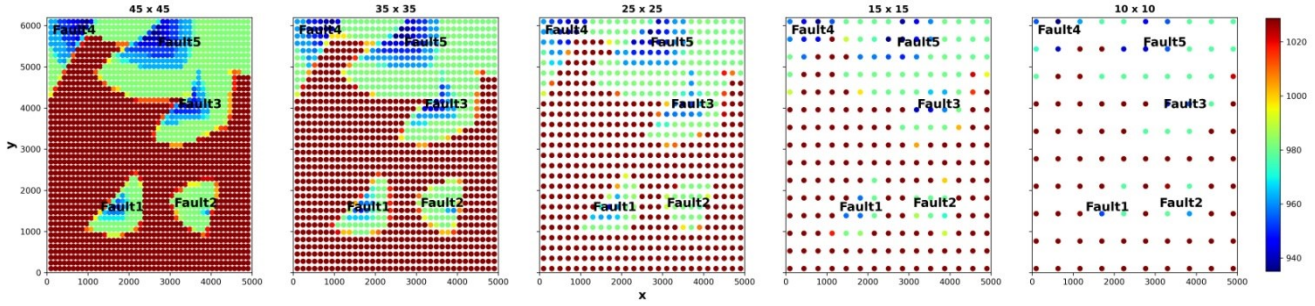

Figure 3: Simulated magnetic data in plan view over the synthetic geological fault model (Figure 1) for different acquisition scenarios- (a) 45x45, (b) 35x35, (c) 25x25, (d) 15x15, and (e) 10x10 acquisition grids.

In this paper, we inverted gravity and magnetic data simulated over a synthetic geological fault model using genetic algorithm, differential evolution, grey wolf optimizer, and particle swarm optimizer to quantify uncertainty in the estimated lithological and fault parameters. The lithology, layer, and fault properties of the synthetic earth model were inspired by the Bradys geothermal field located in the northern part of the Hot Springs Mountains in Nevada. The geology of Bradys is characterized by thick sections of sedimentary and volcanic rocks of Miocene age, underlain by Oligocene ash flow tuffs (Faulds et al., 2003; Witter et al., 2016a). The north-northeast-striking, west-northwest-dipping fault zone acts as the controlling structure for the Bradys geothermal field (Faulds et al., 2013). We begin with a brief description of the synthetic fault model, gravity and magnetic data along with its sensitivity analysis, and algorithms used for inversion. This is followed by a discussion on the results obtained by inverting gravity and magnetic dense grid data using the four stochastic global optimizers. Finally, we analyze the impact that sparse data can have in comparison to dense data on the estimated model parameters from gravity and magnetic data inversion.

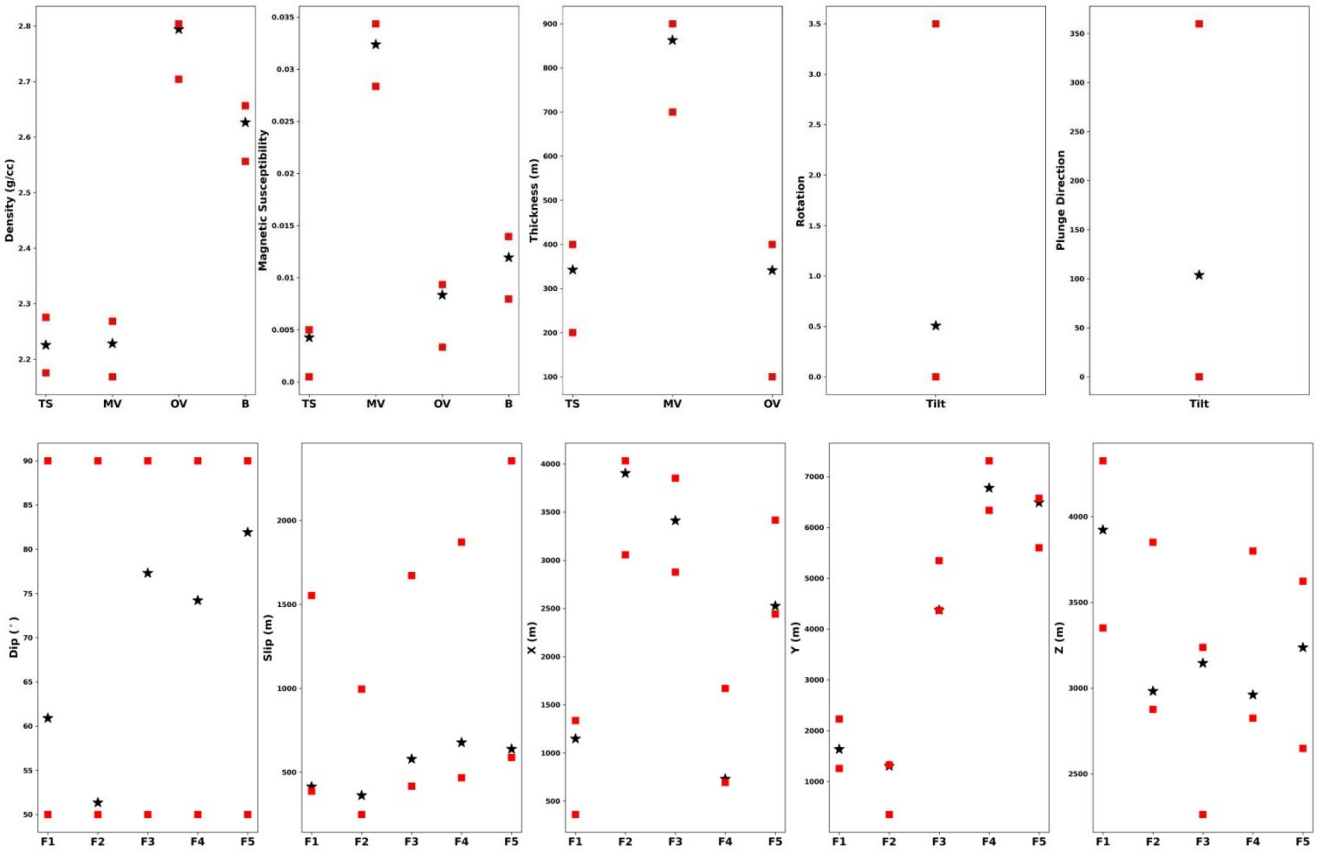

Figure 4: Some of the important model parameters (density and magnetic susceptibility of the four layers, thickness of first three layers, tilt rotation and direction of the geological system, and dip, slip, X-, Y-, Z- coordinate of center of the five faults) used to generate the geological fault model (Figure 1), gravity (Figure 2), and magnetic signatures (Figure 3) with their true values (black star) and uniform bounds (red squares) used for inversion. TS - Tertiary Sediments, MV- Miocene Volcanic, OV- Oligocene Volcanic, B- Basement, F1-Fault 1, F2- Fault2, F3- Fault 3, F4- Fault4, F5- Fault 5.

2. METHODOLOGY

We made use of a kinematic structural modeling software- PyNoddy (Wellmann et al., 2016), a python wrapper for the software Noddy (Jessell and Valenta, 1996) to generate a synthetic four-layered (namely- Tertiary sediments, Miocene volcanic, Oligocene volcanic and basement) five fault (namely- Fault1, Fault2, Fault3, Fault4, and Fault5) geological earth model shown in Figure 1. The Noddy algorithm works by starting with a discretized layered earth model followed by a series of geologic deformation events. We used PyNoddy for generating the fault models because kinematic simulations strike a balance between geologic realism and computational speed. Moreover, Pynoddy can forward simulate gravity and magnetic signatures over a geologic fault model given the layer properties and fault parameters. The simulated gravity and magnetic data over the synthetic fault model (Figure 1) are shown in Figures 2 and 3 respectively. Some of the important model parameters used to generate the structural model (Figure 1), gravity (Figure 2) and magnetic signatures (Figure 3) are shown in Figure 4 along with the uniform priors (bounds) used later for the inversion. The set of model parameters include density, magnetic susceptibility, and thickness of each layer, stratigraphy tilt parameters (the geological system is tilted prior to faulting in Noddy) like the rotation and direction of tilting, and a number of fault parameters like fault location, deformation ellipse properties, dip, dip direction, and slip on each fault. Distance-based global sensitivity analysis of gravity (Figure 5a) and magnetic data (Figure 5b) was also performed to infer the parameters to which the potential field data are sensitive, and a reduction in uncertainty can be expected post-inversion. Not surprisingly, the gravity data is highly sensitive to the density of the layers, while the magnetic data is highly sensitive to magnetic susceptibility of the layers so the priors (bounds) for density and magnetic susceptibility of the layers were well constrained (Figure 4) to get good predictions for geological and fault parameters as well.

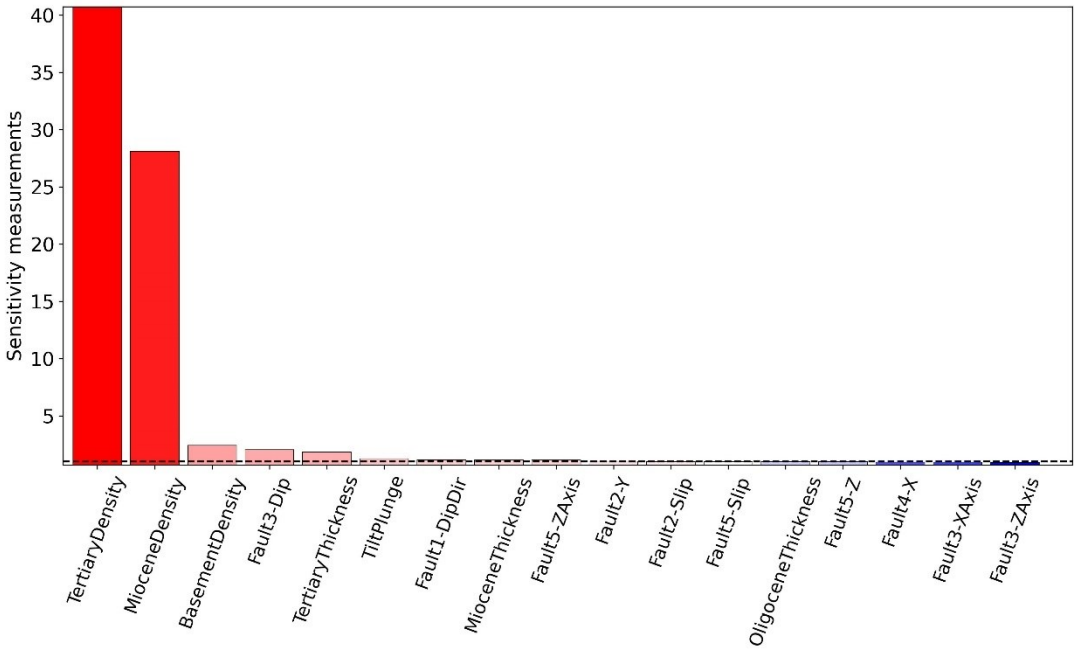

Figure 5a: Distance-based global sensitivity analysis of gravity data to find the model parameters to which gravity data is most sensitive.

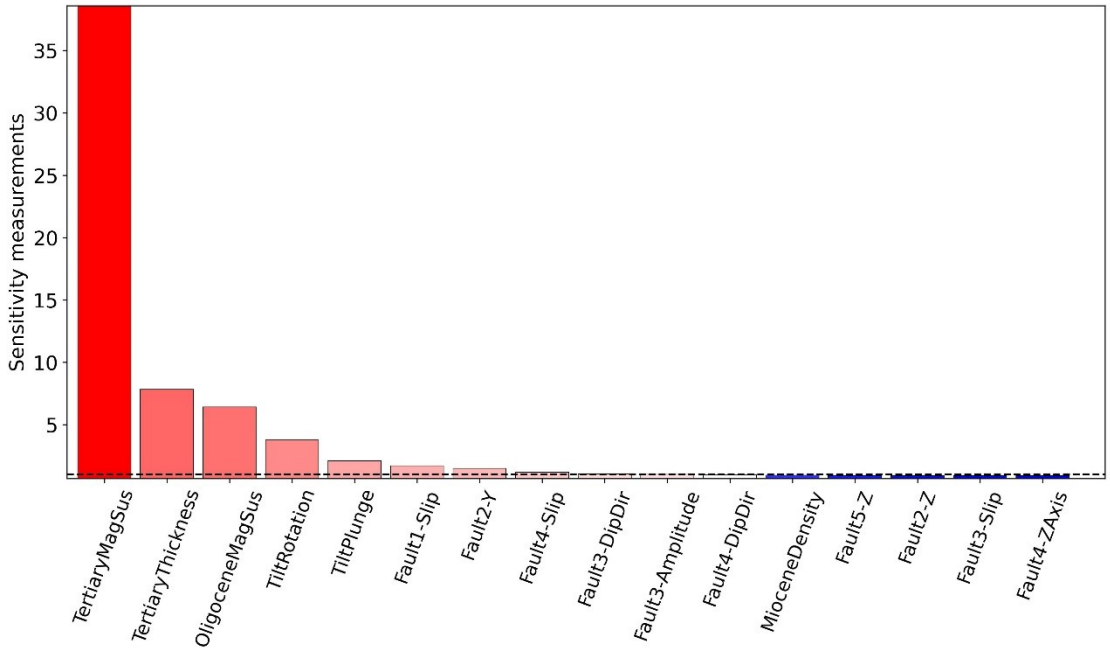

Figure 5b: Distance-based global sensitivity analysis of magnetic data to find the model parameters to which magnetic data is most sensitive.

We inverted gravity and magnetic data using two evolution-inspired (genetic algorithm and differential evolution) and two swarm intelligence-inspired (grey wolf optimization and particle swarm optimization) global optimization techniques. Genetic algorithm (GA) is a stochastic population-based method where the next generation is created from the current generation using a roulette wheel selection mechanism followed by crossover and mutation strategies. Differential evolution (DE) is also a stochastic population-based method where the next generation (trial candidate) is computed by mixing two or more candidate solutions of the current generation using a mutation factor. Particle swarm optimizer (PSO) is a swarm intelligence-inspired technique that loosely mimics flocking behavior of birds or fishes, while grey wolf optimizer (GWO) is inspired by the hunting mechanism of grey wolves. The number of search agents was 20 for both GWO and PSO. Similarly, the population size was also 20 for both GA and DE. All the four stochastic global optimizers were allowed to run for 200 iterations and executed 50 times with different random number generator seeds to get an ensemble of solutions with low misfit error. Root mean square (RMS) error between the "true" computed synthetic and gravity and magnetic signatures computed for each member of the ensemble was minimized to perform the inversion.

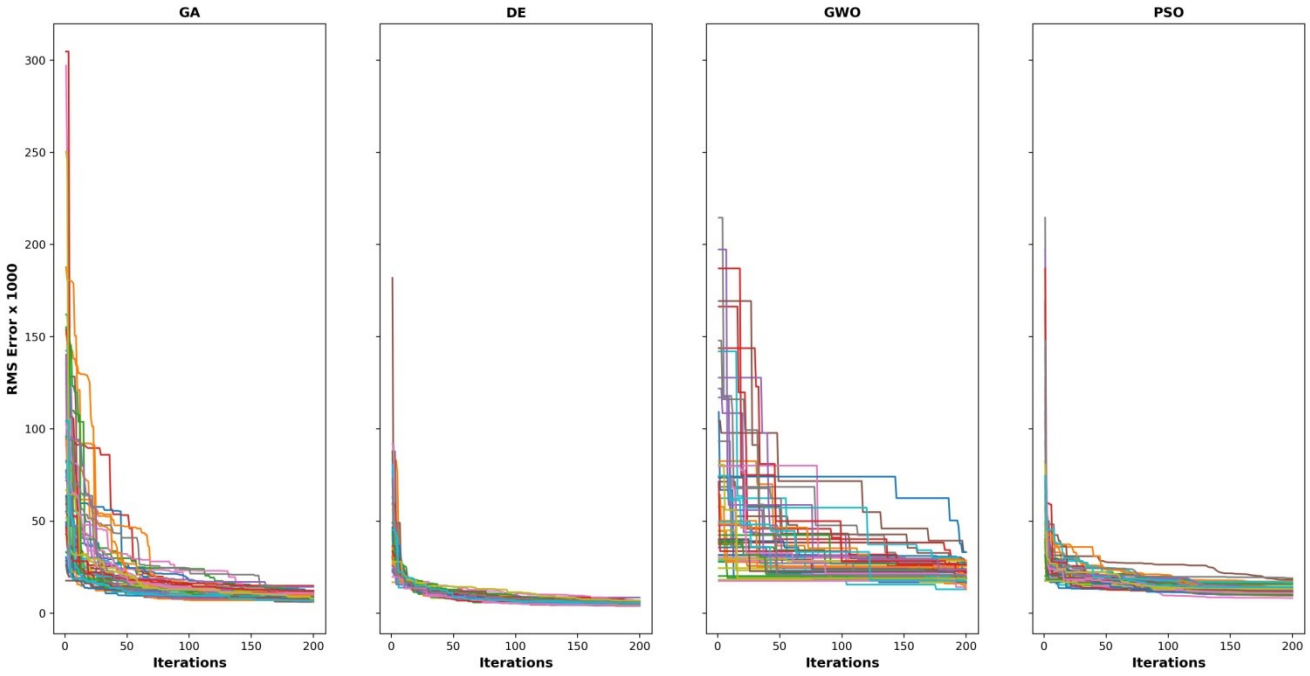

Figure 6: The misfit versus iterations curves of all the 50 simulations for the four stochastic global optimizers (a) GA, (b) DE, (c) GWO, and (d) PSO from gravity data inversion.

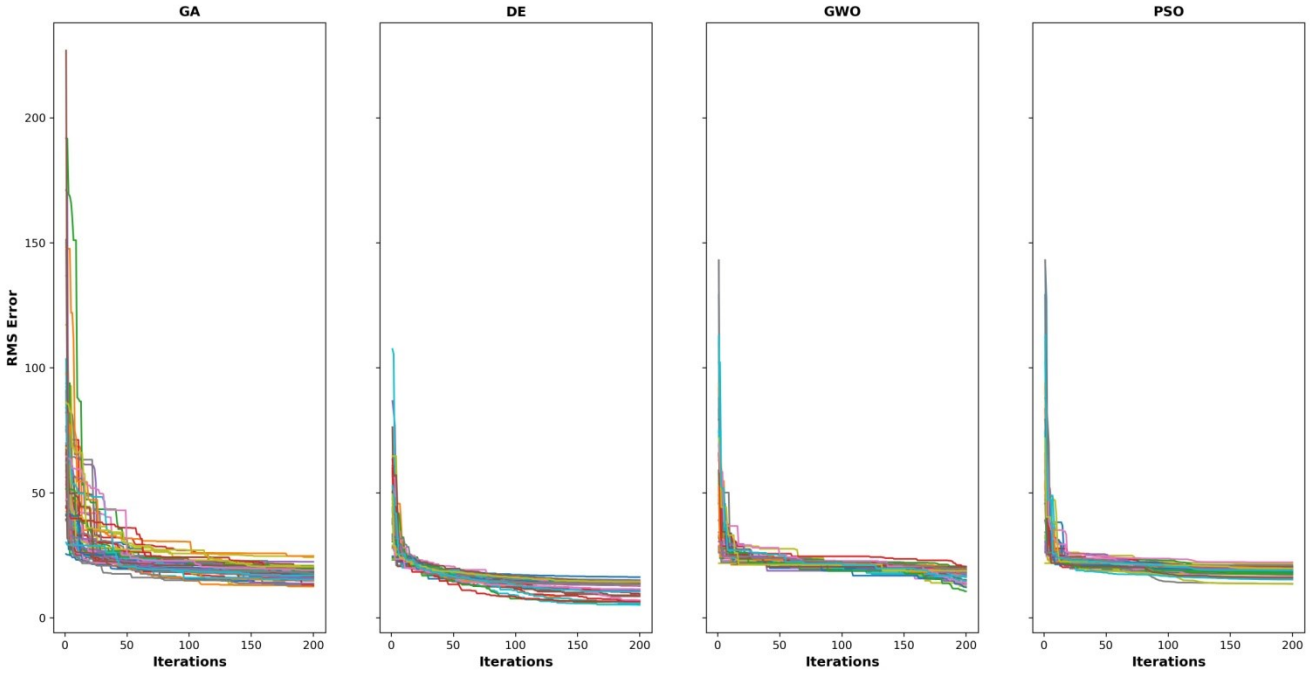

Figure 7: The misfit versus iterations curves of all the 50 simulations for the four stochastic global optimizers (a) GA, (b) DE, (c) GWO, and (d) PSO from magnetic data inversion.

3. GRAVITY AND MAGNETIC DENSE GRID INVERSION

The simulated gravity (Figure 2a) and magnetic (Figure 3a) dense grid (45x45 data points) data were inverted using GA, DE, GWO, and PSO. The misfit versus iterations curves from all four algorithms for gravity and magnetic data are shown in Figures 6 and 7 respectively. A threshold (less than 0.0051 units for gravity and less than 9 units for magnetic) was applied to only keep the models that have very low RMS misfit (match well with the observed "true" data). It was observed that only the models predicted by DE were able to satisfy the threshold (Figure 8), and the models estimated by other global optimizers were unable to pass the threshold. Hence, DE outperformed GA, GWO, and PSO for inversion of gravity and magnetic data, and was used for all the forthcoming comparisons. The

box plot for the model parameters (Figure 4) predicted by DE after gravity and magnetic data inversion are shown in Figures 9a and 9b respectively. For the remainder of the model parameters, uncertainty was not reduced, i.e., the posterior distribution was similar to the prior. The results of gravity data inversion demonstrate a reduction in uncertainty for the following model parameters- density and thickness of Tertiary sediments and Miocene volcanic layer; the tilt rotation of the geological system (the flat stratigraphy is rotated prior to faulting in Noddy); dip of fault 5; slip of faults 2, 3, 4 and 5; the X- and Y-coordinate of the center of faults 2, 3, and 5; the Z-coordinate of the center of fault 1.The results of magnetic data inversion demonstrate a reduction in uncertainty for the following model parameters- magnetic susceptibility and thickness of Tertiary sediments and Miocene volcanic layer; the tilt direction and tilt rotation of the geological system; dip and slip of all the five faults; the X- and Y-coordinate of the center of all the five faults; the Z-coordinate of the center of faults 1, 2, 3, and 5. It should be noted that both gravity and magnetic data inversion results agree with the sensitivity analysis predictions, i.e., the parameters to which data are highly sensitive show reduced uncertainty/narrower posterior distributions. Next, we explore the effects of sparse data acquisition.

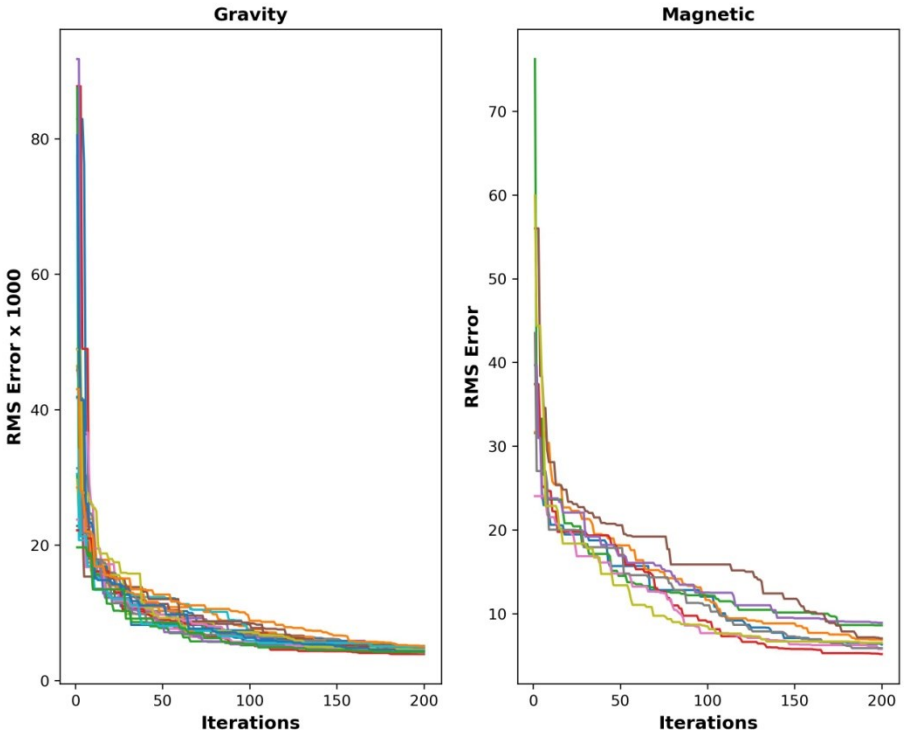

Figure 8: The misfit versus iterations curves for DE from (a) gravity and (b) magnetic data inversion after applying suitable thresholds.

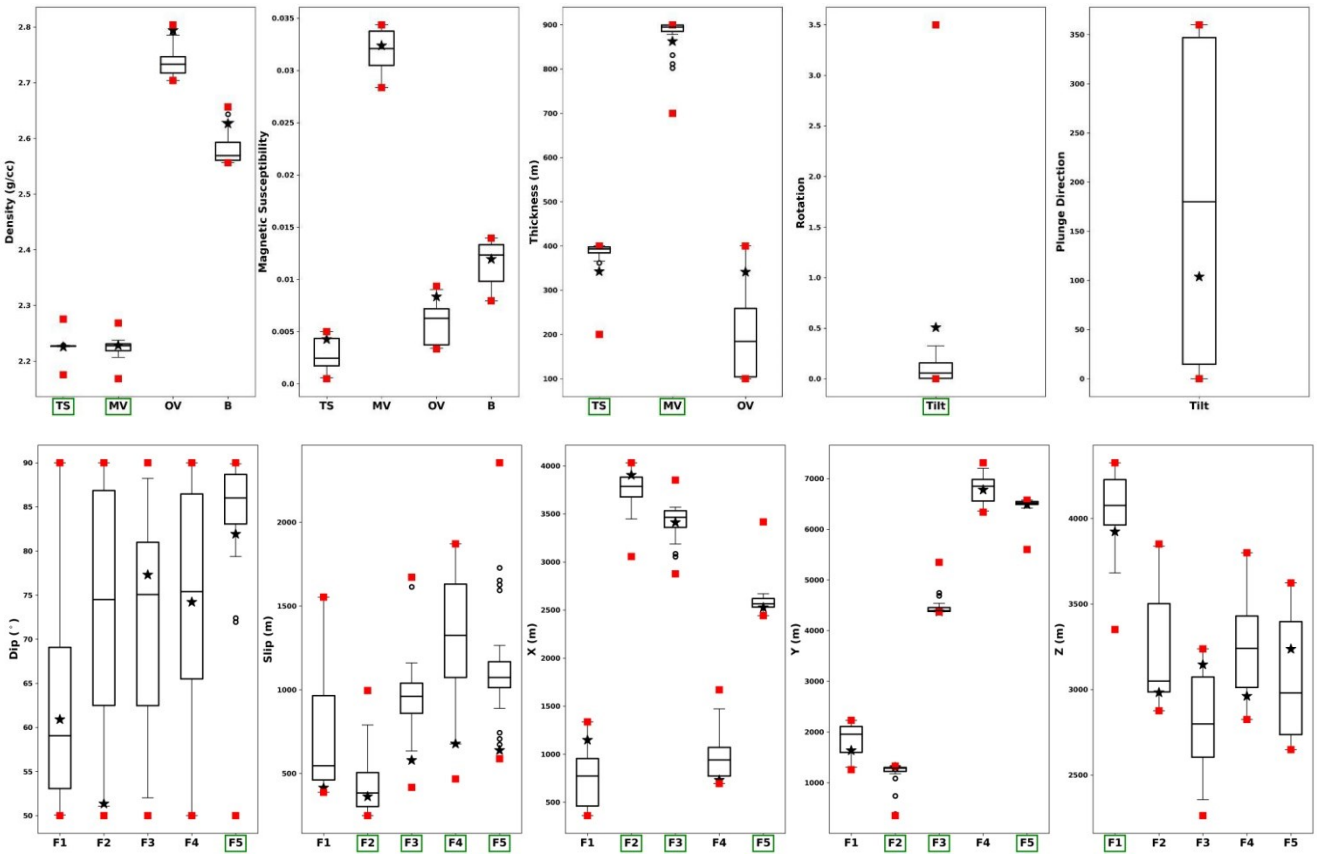

Figure 9a: The box plot of model parameters estimated by DE from inversion of dense grid (45x45) gravity data. The black star indicates the "true" value, the red dots indicate the initial prior uniform bounds, and the box plots show the distributions after the inversions. The parameters with reduced uncertainty are highlighted by green boxes. TS- Tertiary Sediments, MV- Miocene Volcanic, OV- Oligocene Volcanic, B- Basement, F1-Fault 1, F2- Fault2, F3- Fault 3, F4- Fault4, F5- Fault 5.

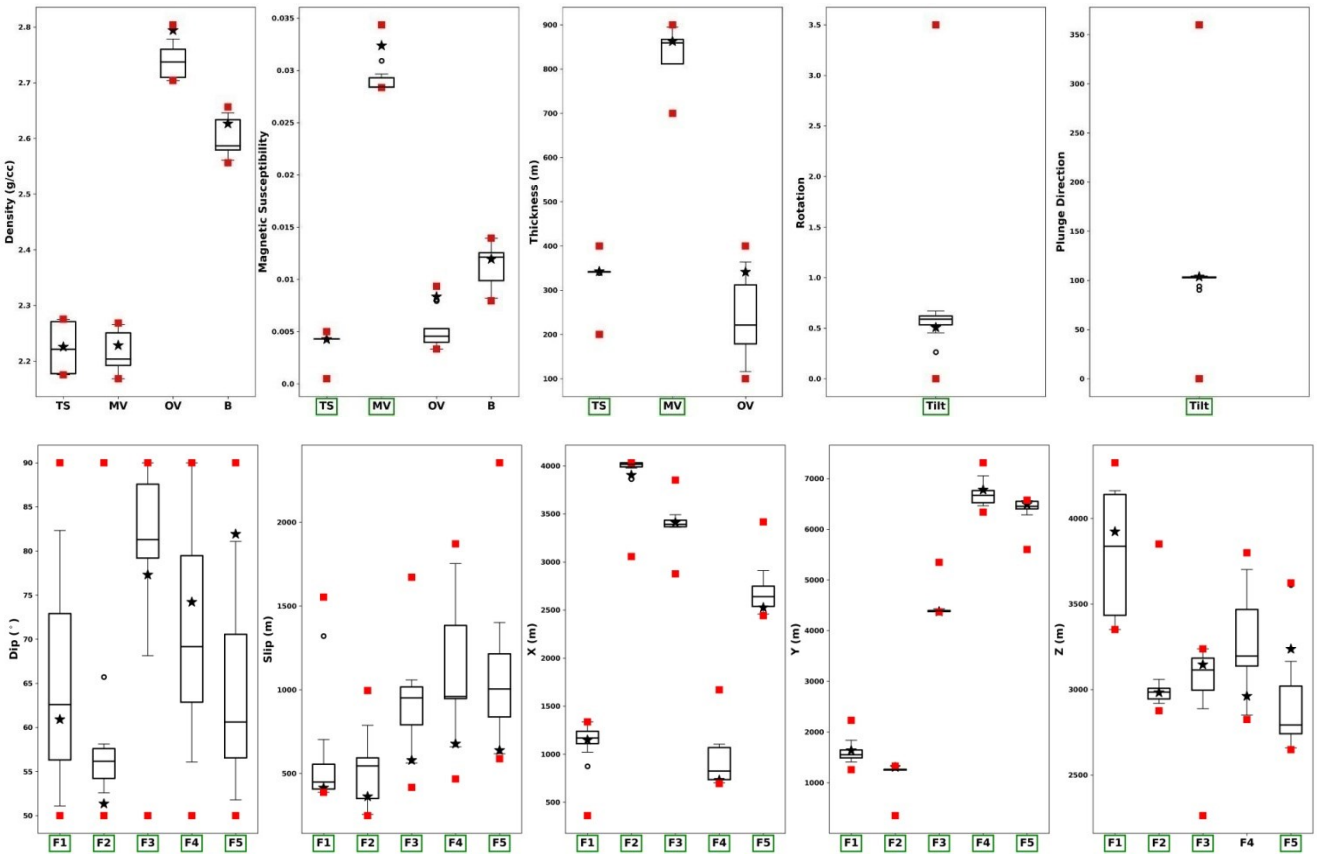

Figure 9b: The box plot of model parameters estimated by DE from inversion of dense grid (45x45) magnetic data. The black star indicates the "true" value, the red dots indicate the initial prior uniform bounds, and the box plots show the distributions after the inversions. The parameters with reduced uncertainty are highlighted by green boxes. TS- Tertiary Sediments, MV- Miocene Volcanic, OV- Oligocene Volcanic, B- Basement, F1-Fault 1, F2- Fault2, F3- Fault 3, F4- Fault4, F5- Fault 5.

4. GRAVITY DENSE AND SPARSE GRID INVERSION

Though gravity and magnetic surveys are economical, acquiring such dense data (Figures 2a and 3a) may not always be possible. For a variety of reasons, it is necessary to study the impact of acquiring sparse data on uncertainty quantification, in comparison to dense grid. Figure 2 displays simulated gravity data for five different acquisition scenarios ranging from dense grid (45x45) to sparse grid (10x10). In Figure 2a (45x45 grid), all the faults (except fault 1) are clearly visible in the gravity data itself. Fault 1 is not visible because the density contrast between the top two layers is not significant. Moreover, it is the deepest (center of the fault) of the five faults with the second lowest slip along the fault, and the displacement is maximum near the center of the fault. Fault 2 can be seen on the gravity data grid but with less amplitude because it has the smallest slip, with the center much closer to the surface. The RMS misfit curves of DE for all five acquisition scenarios after applying the same threshold are shown in Figure 10. Similar results are observed for the dense (45x45) and sparse (10x10) grid acquisition cases (Figure 11), with some increase in uncertainty (widening of posterior) with grid sparsity for some of the model parameters. As there is not a very significant difference between the posteriors of dense and sparse grid inversion results, sparse data acquisition may be preferred, being more economical and feasible.

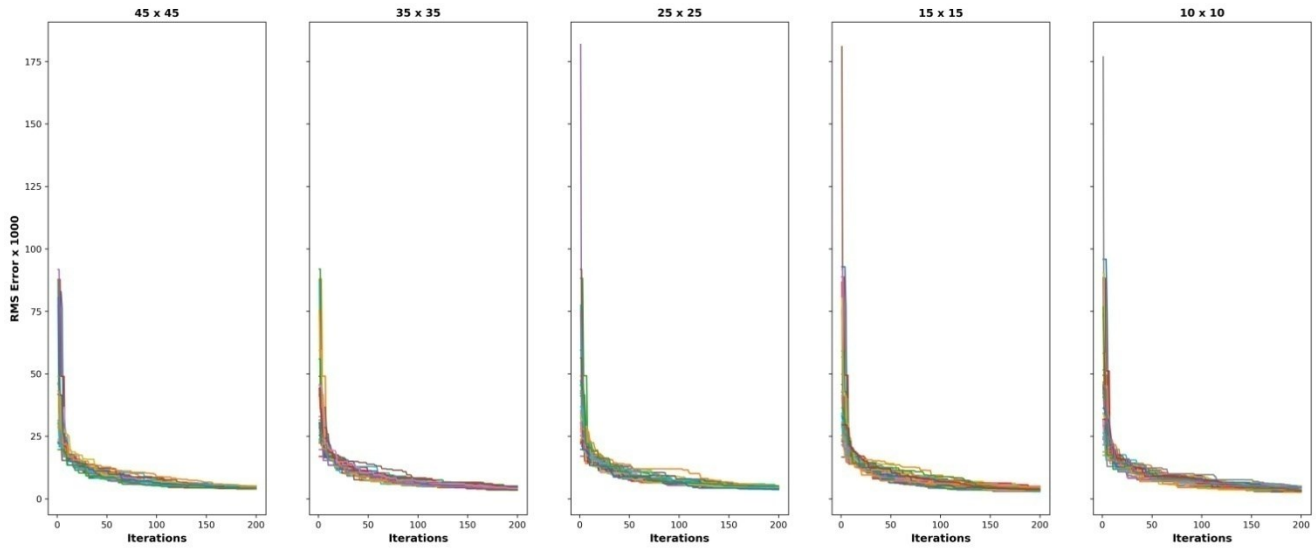

Figure 10: The misfit versus iterations curves for DE from different gravity data acquisition scenarios- (a) 45x45, (b) 35x35, (c) 25x25, (d) 15x15, and (e) 10x10 acquisition grids after applying a suitable threshold.

5. MAGNETIC DENSE AND SPARSE GRID INVERSION

Similar to gravity, we simulated magnetic data (Figure 3) for five different acquisition scenarios ranging from dense grid (45x45) to sparse grid (10x10). Unlike gravity data, all five faults are clearly visible on the magnetic data grid (Figure 3a-c) because of a significant magnetic susceptibility contrast between the Tertiary sediments and Miocene volcanic layer. The RMS error curves of DE for all the acquisition cases after applying the same threshold are shown in Figure 12. Similar results are observed for the dense (45x45) and sparse (10x10) grid acquisition scenarios (Figure 13), with an increase in uncertainty with grid spacing for some of the model parameters. There is some difference between the posteriors of model parameters estimated from dense and sparse data, but the difference may not be remarkable enough to choose a costlier and less feasible dense survey.

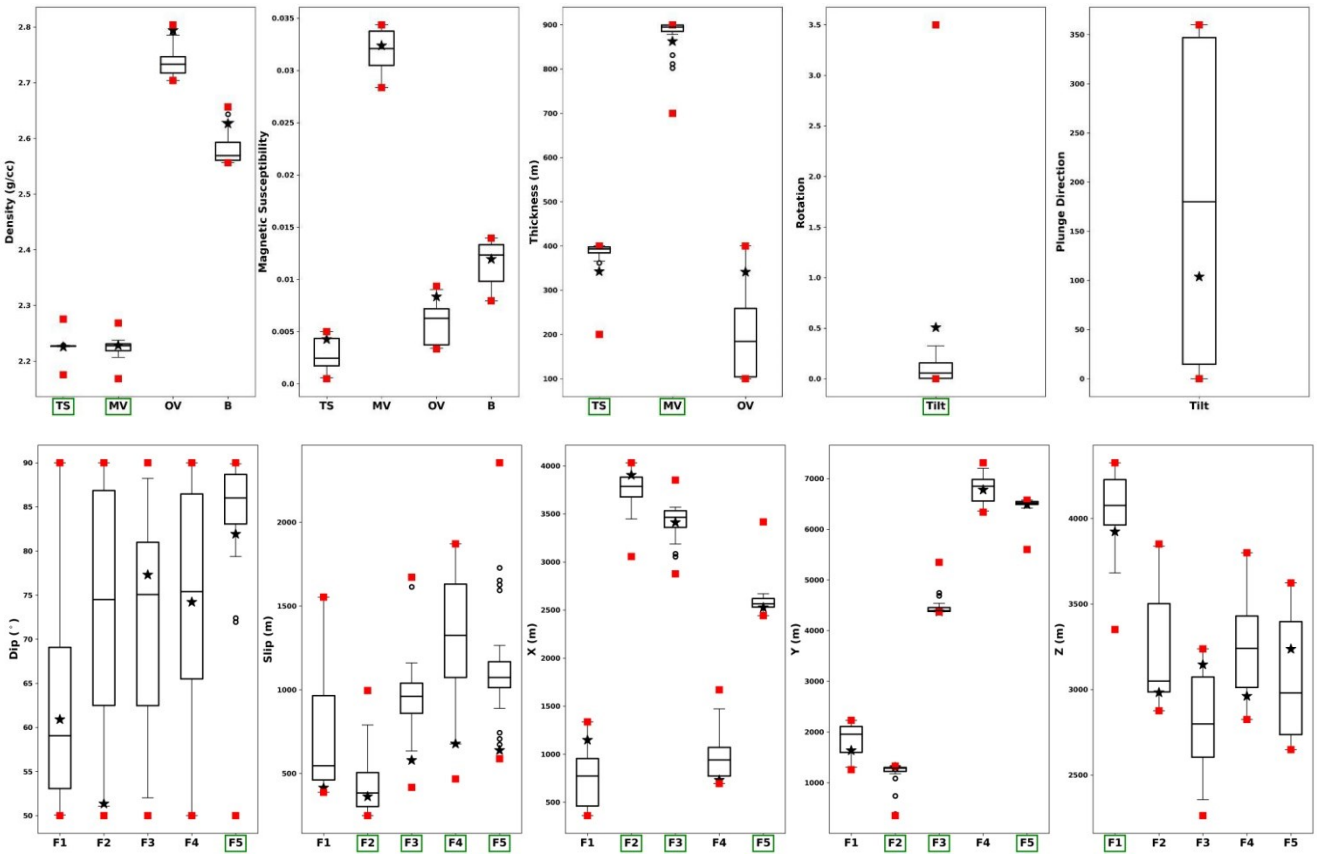

Figure 11a: The box plot of model parameters estimated by DE from inversion of gravity 45x45 grid data. The black star indicates the "true" value, the red dots indicate the initial prior uniform bounds, and the box plots show the distributions after the inversions. The parameters with reduced uncertainty are highlighted by green boxes. TS- Tertiary Sediments, MV- Miocene Volcanic, OV- Oligocene Volcanic, B- Basement, F1-Fault 1, F2- Fault2, F3- Fault 3, F4- Fault4, F5- Fault 5.

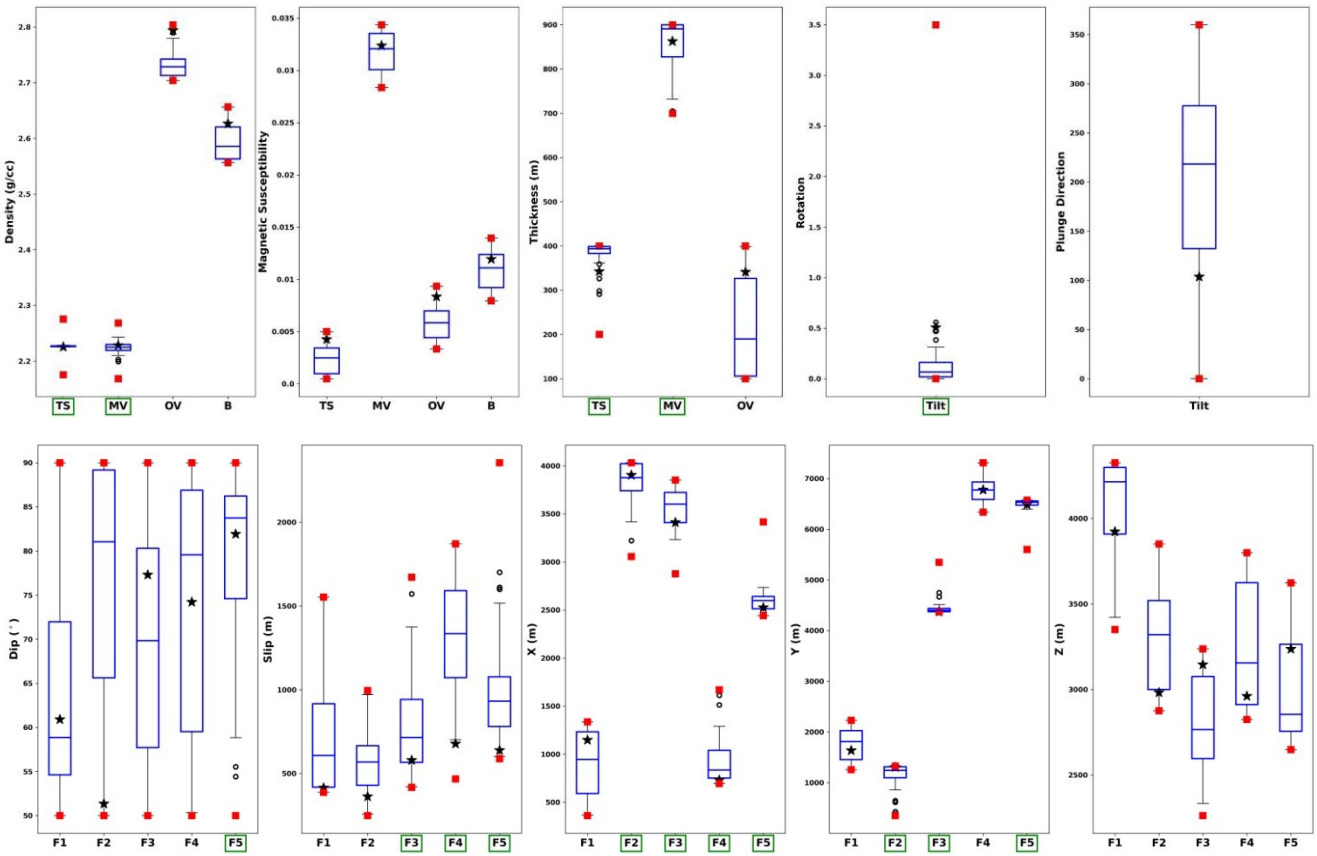

Figure 11b: The box plot of model parameters estimated by DE from inversion of gravity 10x10 grid data. The black star indicates the "true" value, the red dots indicate the initial prior uniform bounds, and the box plots show the distributions after the inversions. The parameters with reduced uncertainty are highlighted by green boxes. TS- Tertiary Sediments, MV- Miocene Volcanic, OV- Oligocene Volcanic, B- Basement, F1-Fault 1, F2- Fault2, F3- Fault 3, F4- Fault4, F5- Fault 5.

6. DISCUSSION

In this paper, we inverted noise-free synthetic gravity and magnetic data to estimate the lithological, and fault parameters of a synthetic four-layered, five-fault earth model. The same forward model was used to compute the synthetic data as well as in the predicted data during the inversion. Both the geophysical surveys were inverted independent of each other, so the next step is to perform joint inversion of the two datatypes to get more robust and confident results. Moreover sequential inversion such as gravity followed by magnetic or vice versa can be attempted to achieve better results. For some of the model parameters their posterior distributions were similar to the prior, so other data types like lithology observed in wells, tracer, and fault marker data can be incorporated in the workflow to compute more realistic geological structural models. Moreover, application to field data is an essential part of this research so the future work will include inversion of the publicly available data from Bradys geothermal field to generate subsurface geological fault models. In this study, we assumed that the number of faults is known which is not a common scenario and is itself an uncertain parameter, so the effect of the uncertainty about the number of faults on the results needs to be analyzed. Pynoddy has its own issues like generating unrealistic earth models (faults cutting and crossing each other, etc.) during forward modeling so different kinematic structural modeling software or physical process simulator can also be used. The run time for a single simulation (gravity, magnetic, and geological fault model) was 0.5 seconds on a single NVIDIA A100 SXM4 GPU. The codes of the stochastic global optimizers used for inversion were adapted from EvoloPy toolbox (Hossam et al., 2016; Khurma et al., 2020).

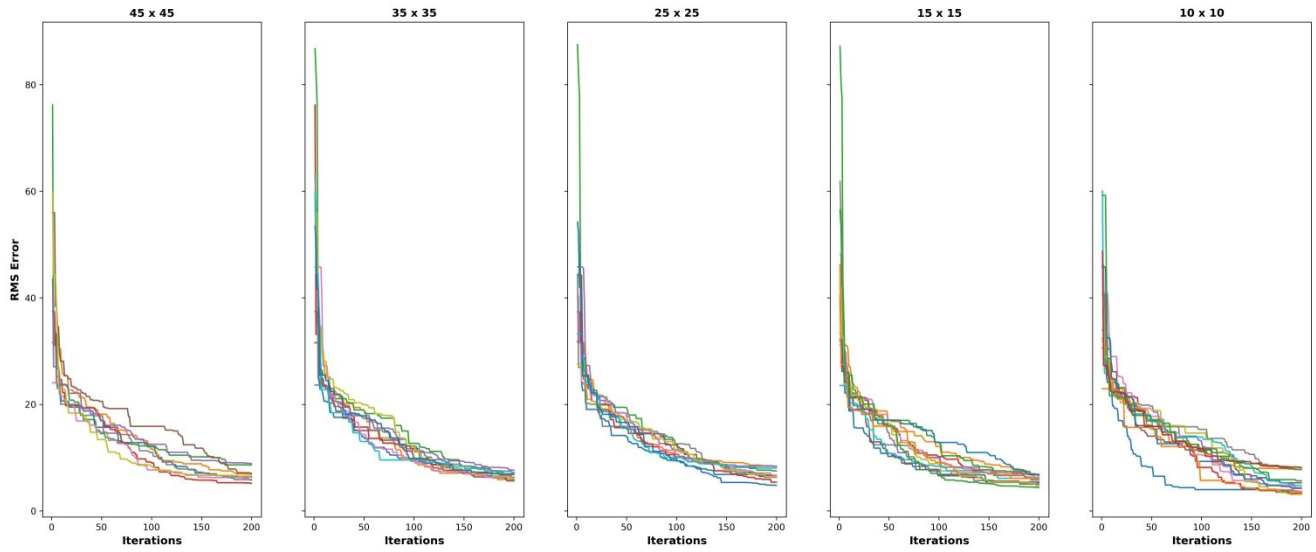

Figure 12: The misfit versus iterations curves for DE from different magnetic data acquisition scenarios- (a) 45x45, (b) 35x35, (c) 25x25, (d) 15x15, and (e) 10x10 acquisition grids after applying a suitable threshold.

7. CONCLUSIONS

We inverted potential field data simulated over a synthetic four-layered, five-fault earth model using four well-known stochastic global optimizers- genetic algorithm, differential evolution, grey wolf optimizer, and particle swarm optimizer. Differential evolution performed the best in all the cases studied giving models with the least RMS misfit. The inversion results stand in agreement with the sensitivity analysis predictions, with the least uncertain (narrow posterior) parameters being those to which the data are highly sensitive. Similar results are observed for all the acquisition scenarios with widening of posterior with sparsity for some of the model parameters. The increase in uncertainty may not be significant enough to choose a costlier and less practicable dense survey. Sparse data acquisition may prove to be a workable solution given the financial restrictions of geothermal field development. It should be noted that the data should not be too sparse that all the necessary information is lost and uncertainty is not reduced post inversion. Although both the geophysical surveys have their own advantages, if only one survey can be performed, it might appear that magnetic data is more valuable than gravity because overall the posteriors are narrower from magnetic data inversion. However these observations are for noise-free data. One of the possible reasons for this observation is the significant magnetic susceptibility contrast between the top two layers in opposition to gravity, where the density contrast is not remarkable. Another reason could be the number of solutions that satisfy the threshold for gravity and magnetic. The numbers of models were about 25 and 12 for gravity and magnetic respectively, so more simulations may lead to a slight broadening of posteriors from magnetic data inversion.

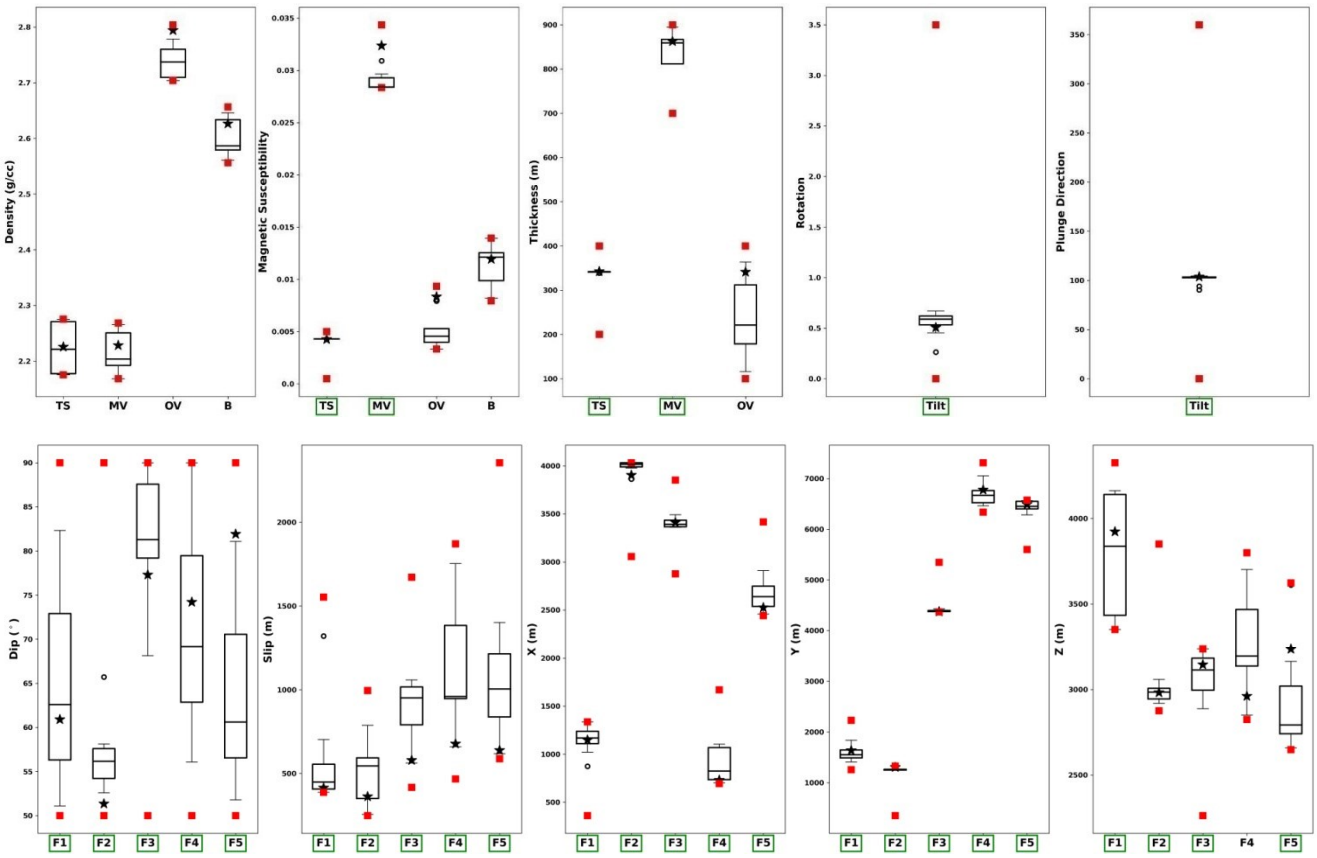

Figure 13a: The box plot of model parameters estimated by DE from inversion of magnetic 45x45 grid data. The black star indicates the "true" value, the red dots indicate the initial prior uniform bounds, and the box plots show the distributions after the inversions. The parameters with reduced uncertainty are highlighted by green boxes. TS- Tertiary Sediments, MV- Miocene Volcanic, OV- Oligocene Volcanic, B- Basement, F1-Fault 1, F2- Fault2, F3- Fault 3, F4- Fault4, F5- Fault 5.

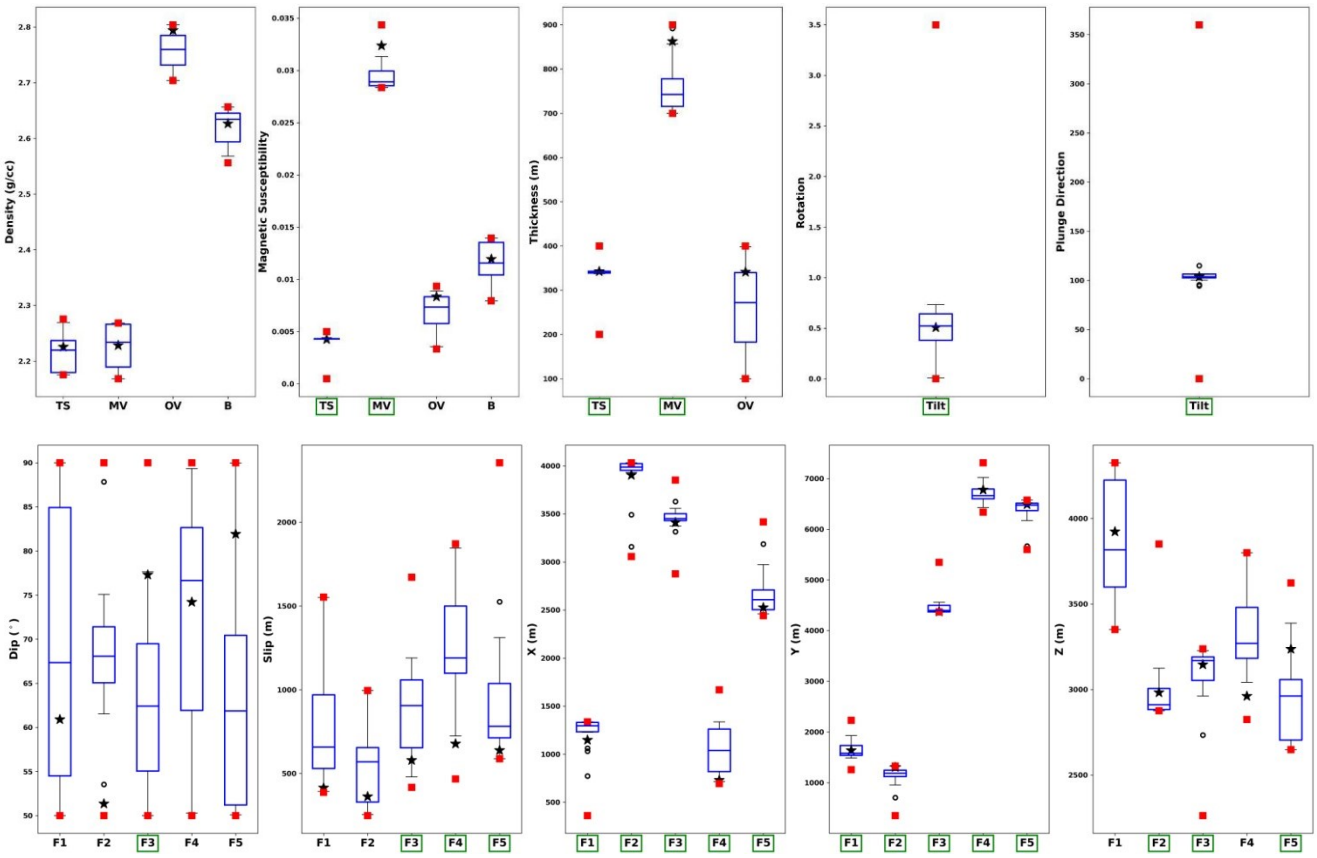

Figure 13b: The box plot of model parameters estimated by DE from inversion of magnetic 10x10 grid data. The black star indicates the "true" value, the red dots indicate the initial prior uniform bounds, and the box plots show the distributions after the inversions. The parameters with reduced uncertainty are highlighted by green boxes. TS- Tertiary Sediments, MV- Miocene Volcanic, OV- Oligocene Volcanic, B- Basement, F1-Fault 1, F2- Fault2, F3- Fault 3, F4- Fault4, F5- Fault 5.

8. ACKNOWLEDGEMENTS

This work is supported by the Stanford Center for Earth Resources Forecasting, and the Stanford Energy Science and Engineering Department.

REFERENCES

Abdelazeem, M., Gobashy, M., Khalil, M.H., and Abdrabou, M.: A complete model parameter optimization from self-potential data using Whale algorithm, Journal of Applied Geophysics, 170, (2019), 103825.

Agarwal, A., Shalivahan, S., Chandra, A. and Singh, R.K.: Grey wolf optimiser: a new strategy to invert geophysical data sets. Geophysical Prospecting, 66(6), (2018), 1215–1226.

Ardestani, V.E., Fournier, D. and Oldenburg, D.W.: Gravity and Magnetic Processing and Inversion Over the Mahallat Geothermal System Using Open Source Resources in Python, Pure Appl. Geophys,.178, (2021), 2171–2190.

Baillieux, P., Schill, E., Edel, J.P. and Mauri, G.: Localization of temperature anomalies in the Upper Rhine Graben: insights from geophysics and neotectonic activity, Int. Geol. Rev., 55(14), (2013), 1744–1762.

Balkaya, Ç.: An implementation of differential evolution algorithm for inversion of geoelectrical data, Journal of Applied Geophysics, 98, (2013), 160–175.

Beaty, K. S., Schmitt, D. R., and Sacchi, M.: Simulated annealing inversion of multimode Rayleigh wave dispersion curves for geological structure, Geophysical Journal International, 151(2), (2013), 622–631.

Calderón, J.P., and Gallardo, L.A.: 3D Convolution Conjugate Gradient Inversion of Potential Fields in Acoculco Geothermal Prospect, Mexico, Front. Earth Sci., 9:759824, (2022). doi: 10.3389/feart.2021.759824

Carrillo, J., Perez, F., Marco, A., Gallardo, L.A. and Schill, E.: Joint inversion of gravity and magnetic data using correspondence maps with application to geothermal fields, Geophys. J. Int., 228(3), (2022), 1621–1636.

Chandra, A., Agarwal, A., Shalivahan, and Singh, R.K.: Grey wolf optimisation for inversion of layered earth geophysical datasets, Near Surface Geophysics, 15, (2017), 499-513.

Faulds, J.E., Garside, L.J., and Oppliger, G.: Structural analysis of the Desert Peak–Brady geothermal fields, northwest Nevada: implications for understanding links between northeast-trending structures and geothermal reservoirs in the Humboldt structural zone, Geotherm Res Counc Trans., 27, (2003), 859–64.

Faulds, J.E., Hinz, N.H., Dering, G.M., and Siler, D.L.: The hybrid model—the most accommodating structural setting for geothermal power generation in the Great Basin, western USA, Geotherm Res Counc Trans., 37, (2013), 3–10.

Grant, F.S. and West, G.F.: Interpretation theory in Applied Geophysics. New York: McGraw Hill Book Company, (1965).

Holland, J.H.:. Adaptation in Natural and Artificial Systems: An Introductory Analysis with Applications to Biology, Control, and Artificial Intelligence. University of Michigan Press, Ann Arbor, MI, (1975).

Hossam, F., Aljarah, I., Mirjalili, S., Castillo, P.A., and Guervós, J.J.M.: EvoloPy: An Open-source Nature-inspired Optimization Framework in Python, In IJCCI (ECTA), 171-177, (2016).

Jessell, M.W. and Valenta, R.K.: Structural geophysics: Integrated structural and geophysical modeling, Comput. Methods Geosci., 15, (1996), 303–324.

Kennedy, J. and Eberhart, R.: Particle swarm optimization. In: International Conference on Neural Networks IV (IEEE) Proceedings, Extended Abstracts, vol. 4. IEEE, (1995), 1942–1948. https: //doi.org/10.1109/ICNN.1995.488968.

Khurma, R.A., Aljarah, I., Sharieh, A. and Mirjalili, S.: Evolopy-fs: An open-source nature-inspired optimization framework in python for feature selection. In Evolutionary Machine Learning Techniques, 131–173, Springer, (2020).

Kirkpatrick, S., Gelatt, C.D. and Vecchi, M.P.: Optimization by simulated annealing, Science, 220(4598), (1983), 671–680, https://doi.org/ 10.1126/science.220.4598.671.

Lewerissa, R., Sismanto, S., Setiawan, A. et al.: Integration of gravity and magnetic inversion for geothermal system evaluation in Suli and Tulehu, Ambon, eastern Indonesia, Arab J Geosci, 13, 726, (2020). https://doi.org/10.1007/s12517-020-05735-7

Li, X. and Yin, M.: Application of differential evolution algorithm on self-potential data, PLoS One 7 (12), 1–11 (e51199), (2012).

Liu, S., Liang, M., and Hu, X.: Particle swarm optimization inversion of magnetic data: Field examples from iron ore deposits in China, GEOPHYSICS, 83, (2018), J43-J59, https://doi.org/10.1190/geo2017-0456.1

Ma, X.Q.: A constrained global inversion method using an overparameterized scheme: Application to poststack seismic data, GEOPHYSICS, 66, (2001), 613-626.

Martínez, J., Gonzalo, E., Álvarez, J. and Kuzma, H.: PSO: A powerful algorithm to solve geophysical inverse problems: Application to a 1D-DC resistivity case, J. Appl. Geophys, 71, (2010), 13–25.

Martinez, C. and Li, Y.: Lithologic characterization using airborne gravity gradient and aeromagnetic data for mineral exploration: a case study in the Quadrilatero Ferrıfero, Brazil, Interpretation, 3(2), (2015), SL1– SL13.

Mirjalili, S., Mirjalili, S.M. and Lewis, A.: Grey wolf optimizer, Advances in Engineering Software, 69, (2014), 46–61.

Mirjalili, S. and Lewis, A.: The whale optimization algorithm, Advances in Engineering Software, 95, (2016), 51–67.

Pace, F., Santilano, A. and Godio, A.: A review of geophysical modeling based on particle swarm optimization, Surveys in Geophysics, 42, (2021), 505–549.

Pan, Z., Liang, H., Gao, Z. and Gao, J.: Differential evolution with subpopulations for high-dimensional seismic inversion, Geophysical Prospecting, 66, (2018), 1060-1069. https://doi.org/10.1111/1365-2478.12620

Pollack, A., Cladouhos, T.T., Swyer, M.W., Siler, D., Mukerji, T. and Horne, R.N.: Stochastic Inversion of Gravity, Magnetic, Tracer, Lithology, And Fault Data for Geologically Realistic Structural Models: Patua Geothermal Field Case Study, Geothermics, 95, (2021), 102129.

Qing, A.: Differential Evolution: Fundamentals and Applications in Electrical Engineering, John Wiley & Sons, New York, (2009).

Ramillien, G.: Genetic algorithms for geophysical parameter inversion from altimeter data, Geophysical Journal International, 147(2), (2001), 393–402.

Roy, A., Dubey, C.P, and Prasad, M.: Gravity inversion for heterogeneous sedimentary basin with b-spline polynomial approximation using differential evolution algorithm, GEOPHYSICS, 86, (2021), F35-F47.

Růžek, B. and Kvasnička, M.: Differential evolution algorithm in the earthquake hypocenter location, Pure Appl. Geophys., 158, (2001), 667–693.

Ryden, N. and Park, C.B.: Fast simulated annealing inversion of surface waves on pavement using phase-velocity spectra, GEOPHYSICS, 71, (2006), R49-R58.

Sambridge, M. and Drijkoningen, G.: Genetic algorithms in seismic waveform inversion, Geophysical Journal International, 109(2), (1992), 323-342.

Saraswat, P., Srivastava, R.P. and Sen, M.K.: Particle swarm and differential evolution —optimization for stochastic inversion of post-stack seismic data, 8th Biennial International Conference & Exposition on Petroleum Geophysics, Hyderabad, India, (2010).

Sen, M.K. and Stoffa, P.L.: Nonlinear one-dimensional seismic waveform inversion using simulated annealing, Geophysics, 56(10), (1991), 1624–1638.

Sen, M.K., Datta-Gupta, A., Stoffa, P.L. et al.: Stochastic reservoir modeling using simulated annealing and genetic algorithm, SPE Formation Evaluation, 10(01), (1995), 49–56. https://doi.org/10.2118/24754-PA.

Serpa, L.F., and Cook, K.L.: Simultaneous inversion modeling of gravity and aeromagnetic data applied to a geothermal study in Utah, GEOPHYSICS, 49, (1984), 1327-1337.

Sharma, A., Vashisth, D., Naresh, B. et al.: An ML scale for Eastern Dharwar Craton and adjoining regions, Journal of Seismology, 25, (2021), 1251–1263.

Shaw, R. and Srivastava, S.: Particle swarm optimisation: a new tool to invert geophysical data, Geophysics, 72(2), (2007), 75–83.

Song, X., Tang, L., Zhao, S., Zhang, X., Li, L., Huang, J. and Cai, W.: Grey wolf optimizer for parameter estimation in surface waves, Soil Dynamics and Earthquake Engineering, 75, (2015), 147–157.

Storn, R. and Price, K.V.: Differential evolution — a simple and efficient adaptive scheme for global optimization over continuous spaces, Technical Report TR-95-012,International Computer Science Institute, Berkeley, (1995).

Storn, R. and Price, K.: Differential evolution — a simple and efficient heuristic for global optimization over continuous spaces, J. Glob. Optim, 11, (1997), 341–359.

Tarantola, A.: Inverse Problem Theory and Methods for Model Parameter Estimation, Society for Industrial and Applied Mathematics, (2005).

Telford, W.M., Geldart, L.P., Sheriff, R.E. and Keys, D.A.: Applied Geophysics, Cambridge, UK: Cambridge University Press, (1976).

Tontini, F.C., de Ronde, C.E., Scott, B.J., Soengkono, S., Stagpoole, V., Timm, C. and Tivey, M.: Interpretation of gravity and magnetic anomalies at Lake Rotomahana: geological and hydrothermal implications, J. Volc. Geotherm. Res., 314, (2016), 84–94.

Vashisth, D., Srivastava, S. and Agarwal, A.: Inversion of potential field data using whale optimisation. In: 88th Annual International Meeting, SEG Technical Program Expanded Abstracts. SEG, (2018), 2828–2832, https://doi.org/10.1190/segam2018-2994811.1.

Vashisth, D. and Shekar, B.: Inversion of Rayleigh-wave phase and group velocity dispersion curves for S-wave velocity by grey wolf optimization. In: EAGE Technical Program Expanded Abstracts. EAGE, (2019), 1–5, https://doi.org/10.3997/2214-4609.201901454.

Vashisth, D., Routa, A.,Mohanty, P.R. and Srivastava, S.: Whale optimization algorithm: a robust strategy to invert geophysical data sets, Abstract presented at 2019 Fall Meeting, AGU, San Francisco, CA. AGU, (2019), NS13B–N0655.

Vashisth, D., Shekar, B. and Srivastava, S.: Joint inversion of Rayleigh wave fundamental and higher order mode phase velocity dispersion curves using multi-objective grey wolf optimization, Geophysical Prospecting, 70, (2022), 479-501.

Wellmann, J.F., Thiele, S.T., Lindsay, M.D. and Jessell, M.W.: Pynoddy 1.0: An experimental platform for automated 3-D kinematic and potential field modeling, Geosci. Model Dev, 9, (2016), 1019–1035.

Witter, J.B., Siler, D.L., Faulds, J.E. and Hinz, N.H.: 3D Geophysical Inversion Modelling of Gravity Data to Test the 3D Geologic Model of the Bradys Geothermal Area, Nevada, USA, Geothermal Energy, v. 4, no. 14, (2016a). doi 10.1186/s40517-016-0056-6.

Witter, J.B., Stelling, P., Knapp, P. and Hinz, N.H.: 3D Geophysical Inversion Modelling of Gravity Data as a Subsurface Geothermal Exploration Tool with an example from Akutan (Alaska, USA), Geothermal Resources Council Transactions, v. 40, (2016b), 647-657.

Witter, J.B., Fournier, D., Schermerhorn, W.D. and Stelling, P.: 3D Geophysical Inversion Modeling of Ground Magnetic Data at Baker Hot Springs, Washington State, USA, Geothermal Resources Council Transactions, v. 41, (2017), 1781-1795.

Xing, Z. and Mazzotti, A.: Two-grid full-waveform Rayleigh-wave inversion via a genetic algorithm – Part 1: Method and synthetic examples, GEOPHYSICS, 84, (2019), R805-R814.

Yin, C. and Hodges, G.: Simulated annealing for airborne EM inversion, GEOPHYSICS, 72, (2007), F189-F195.